Nodal Discontinuous Galerkin Method for Aeroacoustics and Comparison with Finite Difference Schemes

Chen Eryun(陈二云)[1*], *Li Zhi*(李直)[1], *Ma Zunling*(马尊领)[1], *Yang Ailing*(杨爱玲)[1], *Zhao Gaiping*(赵改平)[2]

1. School of Energy and Power Engineering, University of Shanghai for Science and Technology, Shanghai, 200093, P. R. China; 2. School of Medical Instrument and Food Engineering, University of Shanghai for Science and Technology, Shanghai, 200093, P. R. China

(Received 7 May 2013; revised 6 November 2013; accepted 4 May 2014)

Abstract: A nodal discontinuous Galerkin formulation based on Lagrange polynomials basis is used to simulate the acoustic wave propagation. Its dispersion and dissipation properties for the advection equation are investigated by utilizing an eigenvalue analysis. Two test problems of wave propagation with initial disturbance consisting of a Gaussian profile or rectangular pulse are performed. And the performance of the schemes in short, intermediate, and long waves is evaluated. Moreover, numerical results between the nodal discontinuous Galerkin method and finite difference type schemes are compared, which indicate that the numerical solution obtained using nodal discontinuous Galerkin method with a pure central flux has obviously high frequency oscillations for initial disturbance consisting of a rectangular pulse, which is the same as those obtained using finite difference type schemes without artificial selective damping. When an upwind flux is adopted, spurious waves are eliminated effectively except for the location of discontinuities. When a limiter is used, the spurious short waves are almost completely removed. Therefore, the quality of the computed solution has improved.

Key words: nodal discontinuous Galerkin method; dispersion and dissipation errors; spurious waves

CLC number: O354.4 **Document code**: A **Article ID**: 1005-1120(2014)03-0293-10

1 Introduction

The numerical simulation of acoustic wave propagation poses a significant challenge in scientific computation. For simulating such problems directly, numerical schemes that have minimal dispersion and dissipation errors are expected. Since the acoustic waves are non-dispersive and non-dissipative in their propagation[1], it makes standard computational fluid dynamics (CFD) schemes, designed for applications to fluid problems, generally inadequate to simulate acoustic problems. In this regard, it has appeared that highly accurate methods are needed for long-time simulations of acoustic wave propagation phenomena, because they are usually less dispersive and less dissipative.

Many current numerical methods employed to study such problems are the finite difference type, such as the widely used dispersion-relation preserving (DRP) scheme[2,3] and compact scheme[4,5]. But the finite difference scheme is based on uniform Cartesian grid, which does not adapt well to complex geometries. Subsequently, finite element method has also been advocated by numerous authors[6]. This method uses unstructured meshes, but it is still not able to solve Euler's linearized equation without spurious mode[7]. Recently, a discontinuous Galerkin finite element method (DG-FEM) has been developed to numerically solve the initial boundary value associated with hyperbolic conversation equations[8-12]. The method is a finite element method that allows discontinuity of the numerical solution

Foundation items: Supported by the National Natural Science Foundation of China (51106099, 50976072); the Leading Academic Discipline Project of Shanghai Municipal Education Commission (J50501).

* **Corresponding author**: Chen Eryun, Associate Professor, E-mail: cheneryun@usst.edu.cn.

at element interfaces, and has the advantage of being more flexible for complex geometries[13,14]. Coupled with its capacity and relative ease of implementation in high-order polynomials, it has been recognized as an attractive alternative method for acoustic problems[15,16].

According to the differential expression of approximation, there are two distinct types of DG method: nodal and modal[17]. In Ref. [15], a study on modal DG method, which is based on Legendre polynomials basis, to acoustics propagation has been presented and some corresponding works, including dispersive, dissipative characteristics and perfectly matched layer absorbing boundary condition, were discussed in Refs. [16, 18]. Thus in this paper, dispersion and dissipation properties of nodal DG method, which is based on Lagrange polynomials basis, are investigated by utilizing an eigenvalue analysis. Then, some test problems of wave propagation with initial disturbance consisting of a Gaussian profile or rectangular pulse are investigated, and the performance of the method in short, intermediate, and long waves are evaluated. Finally, the comparisons of dispersion properties are performed between the nodal DG method and finite difference type schemes.

2 Description of Nodal DG Method and Its Dispersive Properties

2.1 Model problem

Consider an advection equation in one dimensional space

$$\partial u/\partial t + \partial f/\partial x = 0 \tag{1}$$

where $f = au$, here a is a constant. This is subject to appropriate initial conditions

$$u(x,0) = \exp(\mathrm{i}kx) \tag{2}$$

where $x \in \mathbf{R}$, k is the wave number of the initial condition. It is well-known that Eq. (1) admits non-trivial solutions of the form

$$u(x,t) = \exp[\mathrm{i}(kx - \omega t)] \tag{3}$$

where ω is a prescribed frequency. Inserting Eq. (3) into Eq. (1), one easily recovers that $\omega = ka$, known as the dispersion relation with a being the exact phase velocity.

2.2 Discontinuous Galerkin discretisation

It is assumed that the computational domain splits into non-overlapping equidistant elements, D^n, with uniform grid length, $h = x_{\mathrm{r}}^n - x_{\mathrm{l}}^n$, as shown in Fig. 1, where subscripts "r" and "l" represent the right and left interfaces of the element, respectively.

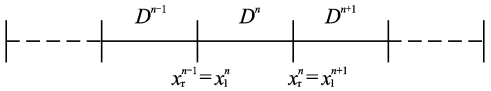

Fig. 1 Geometry for simple one-dimensional case

In Fig. 1, for each element, the local solution approximation, denoted by $u_h^n(x,t)$, with polynomial basis functions is expressed as

$$u_h^n(x,t) = \sum_{p=1}^{m+1} \hat{u}_h^n(x_p,t) l_p^n(x) \tag{4}$$

where $l_p^n(x) \in P_m(D^n)$, $P_m(D^n)$ is the mth order polynomial space on D^n, $l_p^n(x)$, $p = 1, \cdots, m+1$ are Lagrange polynomials defined on $m+1$ interpolating grid points within D^n, then the order of scheme is $m+1$.

In order to determine the approximate solution $u_h^n(x,t)$, Eq. (1) is multiplied by a test function v and integrated over the interval D^n. Then, the exact solution $u(x,t)$ is replaced by the approximation $u_h^n(x,t)$, and the test function v is replaced by v_h^n. After applying the integration by part twice, the strong formulation form is recovered.

$$\int_{D^n} \frac{\partial u_h^n(x,t)}{\partial t} v_h^n(x)\,\mathrm{d}x + \int_{D^n} \frac{\partial f}{\partial x} v_h^n(x)\,\mathrm{d}x = \left[f_h^n(u_h^n) v_h^n(x) - f^*(u_h^n) v_h^n(x) \right]_{x_{\mathrm{l}}^n}^{x_{\mathrm{r}}^n} \tag{5}$$

where numerical flux can be expressed as $f^*(u_h^n) = f^*(u_h^-, u_h^+)$, whose value at the point (x,t) depends on the two values of the approximate solution at (x,t). One u_h^- is the value obtained from the interior of the element D^n, and the other u_h^+ is the value obtained from the exterior of the element D^n. In this paper, the expression of numerical flux is defined as

$$f^* = (au)^* = a\frac{u^- + u^+}{2} + |a|\frac{(1-\alpha)}{2}(\hat{\boldsymbol{n}}^- u^- + \hat{\boldsymbol{n}}^+ u^+) \tag{6}$$

where parameter α in the numerical flux can be used to control dissipation. For example, taking $\alpha=1$ yields a non-dissipative central flux and $\alpha=0$ results in the classic upwind flux[17]. One is free, however, to take α to be any value in between. $\hat{\boldsymbol{n}}$ is a unit outer normal vector.

Assuming that flux $f(u_h^n)=\sum_{p=1}^{m+1} f(\hat{u}_h^n(x_p,t))l_p^n(x)$, test function $v_h^n(x)=\sum_{q=1}^{m+1}\hat{v}_h^n l_q^n(x)$, Eq. (5) is rewritten as

$$\frac{\mathrm{d}\hat{u}_h^n}{\mathrm{d}t}\int_{D^n} l_p^n(x)l_q^n(x)\mathrm{d}x+\int_{D^n} a\hat{u}_h^n\frac{\partial l_p^n(x)}{\partial x}l_q^n(x)\mathrm{d}x=\left[(au_h^n)l_q^n(x)-(au_h^n)^* l_q^n(x)\right]_{x_l^n}^{x_r^n} \tag{7}$$

for all locally defined test functions $\hat{v}_h^n$. Eq. (7) yields a system of time evolution equations for the expansion coefficients for each element. This system is usually solved by some time integration scheme, such as the Runge-Kutta schemes[19].

2.3 Dispersive behaviour of nodal discontinuous Galerkin method

Introducing a local coordinate ξ for each element, and assuming $\xi=\frac{2}{h}\left(x-\frac{x_r^n+x_l^n}{2}\right)$, one has

$$\frac{hM}{2}\frac{\mathrm{d}\hat{u}_h^n}{\mathrm{d}t}+aS\hat{u}_h^n=\frac{a\alpha e_{m+1}}{2}[\hat{u}_h^n(x_r^n,t)-\hat{u}_h^{n+1}(x_l^{n+1},t)]-\frac{a(2-\alpha)e_1}{2}[\hat{u}_h^n(x_l^n,t)-\hat{u}_h^{n-1}(x_r^{n-1},t)] \tag{8}$$

where $M=\int_{-1}^{1} l_p(\xi)l_q(\xi)\mathrm{d}\xi$ is the mass matrix, $S=\int_{-1}^{1} l_p(\xi)\frac{\mathrm{d}l_q(\xi)}{\mathrm{d}\xi}\mathrm{d}\xi$ is the stiffness matrix, and $e_p(p=1,\cdots,m+1)$ is an $m+1$ long zero vector with 1 in entry p.

To compute the dispersion relation of the scheme, a solution is sought in the usual form

$$u_h^n(x,t)=\boldsymbol{U}_h^n\exp[\mathrm{i}(kx-\omega t)] \tag{9}$$

where $\boldsymbol{U}_h^n$ is the vector of coefficients. Eq. (9) represents a sinusoidal wave train in terms of wave number k and frequency ω. Then the expansion coefficients of the solution $\hat{u}_h^n(x_p,t)$ are calculated by projecting Eq. (9) onto the local basis of the elements in the mesh as

$$\hat{u}_h^n(x_p,t)=\boldsymbol{U}_h^n\frac{\int\exp[\mathrm{i}(kx-\omega t)]l_p^n(x)\mathrm{d}x}{\int(l_p^n(x))^2\mathrm{d}x}$$

Assume periodicity of the solution as

$$u_h^{n+1}(x_l^{n+1},t)=\exp(\mathrm{i}kh)u_h^n(x_l^n,t)$$

$$u_h^{n-1}(x_r^{n-1},t)=\exp(-\mathrm{i}kh)u_h^n(x_r^n,t)$$

After isoparametric transforming, and insert them into Eq. (8), one obtains

$$\left[-\frac{\mathrm{i}\omega h}{2}M+aS-\frac{a\alpha}{2}e_{m+1}(e_{m+1}^{\mathrm{T}}-\exp(\mathrm{i}kh)e_1^{\mathrm{T}})+\frac{a(2-\alpha)}{2}e_1(e_1^{\mathrm{T}}-\exp(-\mathrm{i}kh)e_{m+1}^{\mathrm{T}})\right]\boldsymbol{U}_h^n=0 \tag{10}$$

It is recognized as a generalized eigenvalue problem

$$[2S-\alpha e_{m+1}(e_{m+1}^{\mathrm{T}}-\exp(\mathrm{i}L(m+1))e_1^{\mathrm{T}})+(2-\alpha)e_1(e_1^{\mathrm{T}}-\exp(-\mathrm{i}L(m+1))e_{m+1}^{\mathrm{T}})]U_h^n=\mathrm{i}(m+1)\Omega M\boldsymbol{U}_h^n \tag{11}$$

The problem is normalized as

$$L=kh/(m+1),\Omega=\omega h/[a(m+1)]$$

It is found that the numerical dispersion relation is that $L=\Omega$ now, where the values of Ω are generally complex. By solving the generalized eigenvalue problem for $\Omega=\Omega_r+\mathrm{i}\Omega_i$, one obtains the numerical dispersion relation in terms of the real part Ω_r, which is the dispersion associated with the scheme, and the imaginary part Ω_i, which represents the numerical damping inherent in the discretisation process.

The solution of Eq. (11) for a second-order nodal-DG method involves two modes. Fig. 2 shows the dispersion relation of nodal-DG method with the pure upwind flux for these modes, where the solid lines represent the exact case, and the symbol-marked lines represent the numerical dispersion and dissipation properties. One can see that the numerical phase velocity, plotted as the circle lines, is very close to the physical wave speed, up to approximately $L=0.6$ (according to the accuracy limit $|\Omega_r-L|<0.005$). As the normalized wave number increases beyond 0.6, the numerical wave speed starts to deviate from the exact value. Parasite mode associated with the numerical scheme Eq. (8) is shown as the quadrangle lines in Fig. 2. Note that the parasite wave is severely damped for the resolvable range of wave numbers. The directions of propagation of these two numerical modes are opposite.

Fig. 3 shows the dispersion relations of nodal

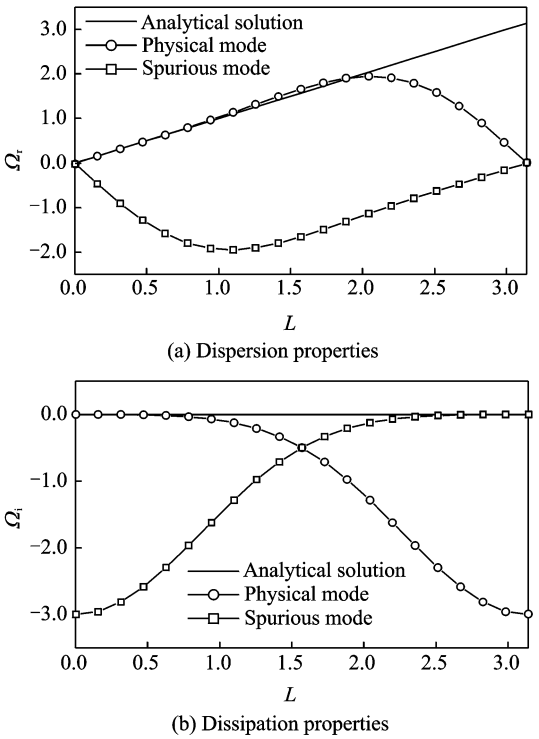

Fig. 2 Numerical dispersion relations for schemes of order 2

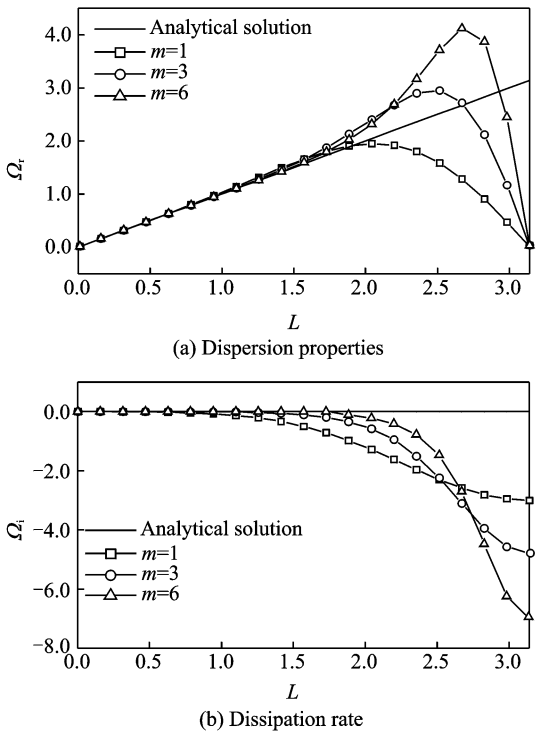

Fig. 3 Numerical dispersion relation and dissipation rate of physical mode for schemes of orders 2, 4 and 7

DG method for the upwind flux with different orders of approximation, where the solid lines represent the exact case, and the symbol-marked lines represent the numerical dispersion relations for a range of orders of approximation. The numerical results indicate that normalized maximum resolvable wave number of the scheme is about 0.62, 1.09 and 1.40 for schemes of orders 2, 4 and 7, respectively, which is according to the criteria mentioned above, i.e., $|\Omega_r - L| < 0.005$. Clearly, the higher the order of the basis functions, the larger the resolved space, which confirms the benefits of using high-order schemes for wave propagation. Moreover, as shown in Fig. 3, Ω_i is for the different orders of approximation, reflecting a significant dissipation of high frequency components.

To quantify the resolution of the scheme, let us specify the dispersion and dissipation errors[16] to be less than 0.5%, i.e., $|\Omega_r - L| < 0.005$ and $|\Omega_i| < 0.005$. The dissipation criterion corresponds to the damping of wave amplitude by less than 10% over a distance of 20 elements. The resolution property of the nodal-DG method is quantified in Table 1 using the maximum resolvable wave number k_c and the number of degrees of freedom per wavelength (computed as $\lambda/(h(m+1))$), according to the accuracy limit ($|\Omega_r - L| < 0.005$ and $|\Omega_i| < 0.005$) on dispersion and dissipation errors. It is evident from Fig. 3 and Table 1 that the limit on the dissipation error imposes a relatively stringent condition on the accuracy of the scheme than does the dispersion error. It is evident that under the higher orders of the scheme, the number of points per wavelength of nodal DG method is less than those of modal DG method shown Table 1 in Ref. [16].

Table 1 Maximum resolvable wave number $k_c h$ according to criteria $|\Omega_r - L| < 0.005$ and $|\Omega_i| < 0.005$

Order (m+1)	$k_c h$	Point number per wavelength
2	0.62	19.94
3	1.88	10.02
4	3.77	6.66
5	5.50	5.71
6	7.54	5.00
9	12.72	4.44
13	20.42	4.00

Fig. 4 shows the comparison of dispersion properties among the nodal DG method, DRP scheme and compact finite difference scheme, where the solid lines represent the exact case; the dot line, the circle line and the triangle line represent the dispersion properties of nodal DG method, DRP scheme and compact scheme, respectively. For convenient comparison, the wave number is normalized by the order of the scheme $m+1$. The numerical results indicate that the normalized maximum resolvable wave number of the scheme is about 1.26, 1.15 and 1.32 for nodal DG method, DRP scheme and compact scheme, respectively, according to the criteria that the absolute errors are less than 0.5%. It illustrates that the nodal DG method is appropriate to direct numerical simulation of aeroacoustics.

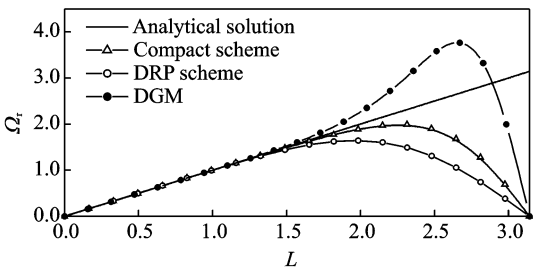

Fig. 4 Comparison of dispersion properties for different numerical schemes with the same orders

3 Numerical Examples

To validate the nodal DG method for acoustics wave propagation, authors consider the solution of advection Eq. (1) with initial disturbance consisting of a Gaussian profile or rectangular pulse[20,21] and let $a=1$. In all cases, grid length is $h=1$.

Example 1 Initial disturbance consisting of Gaussian profile is

$$u(x,0)=\exp[-\ln(2)(x/b)^2] \qquad (12)$$

where b is the parameter that characterizes the wavelength. In this paper, the performance of the DG method in short, intermediate, and long waves is evaluated. That is to say, three categories of waves are considered: (1) short waves ($b=3$); (2) intermediate waves ($b=6$); (3) long waves ($b=20$). Moreover, the comparisons of numerical results between the nodal DG method and the 7-point stencil DRP scheme combined with the fourth-order four-step Runge-Kutta method are performed.

Figs. 5—7 show an overview of the two numerical methods, namely, the nodal DG method and the DRP scheme for short, intermediate, and long wave computation at two different dimensionless time instants, where the circle lines represent the numerical results and the solid lines represent the exact cases. The computed results obtained using DG method and the exact solutions agree well with each other, which indicate that the method produces a small level of dissipation, without dispersion. For the DRP scheme, the characteristics are different for short, intermediate, and long wave computation. For a short wave, the DRP scheme initially produces a lower error level, as shown in Fig. 5(d). At dimensionless time $t=1\,500$, there is significant numerical dispersion (with extensive trailing waves) in Fig. 5(e). As time progresses, dispersion becomes highly visible while dissipation becomes gradually substantial, as shown in Fig. 5(f). For an intermediate wave, throughout the entire computation, only a small dispersion error appears (Fig. 6(d)). For a long wave, DRP scheme performs very well over the interval of time as shown in Fig. 7.

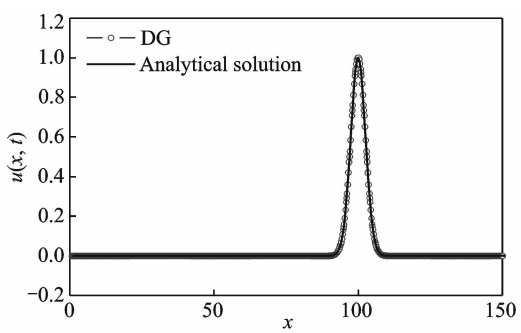

(a) Comparison between exact solutions and DG method (b=3, t=100)

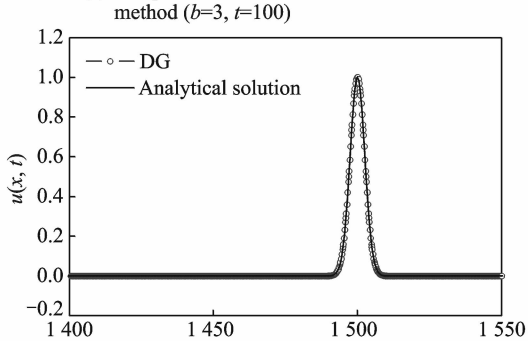

(b) Comparison between exact solutions and DG method (b=3, t=1 500)

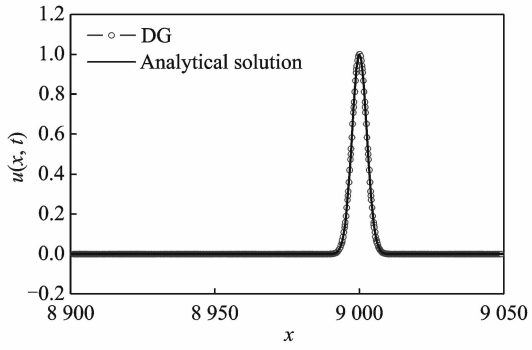

(c) Comparison between exact solutions and DG method (b=3, t=9 000)

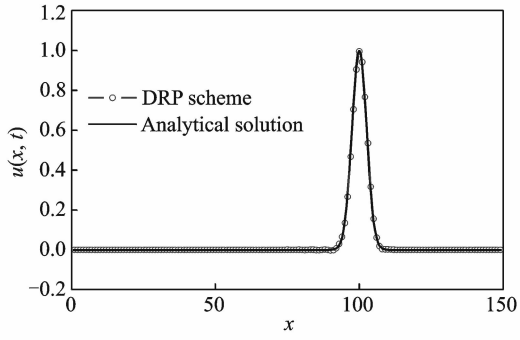

(d) Comparison between exact solutions and DRP scheme (b=3, CFL=1, t=100)

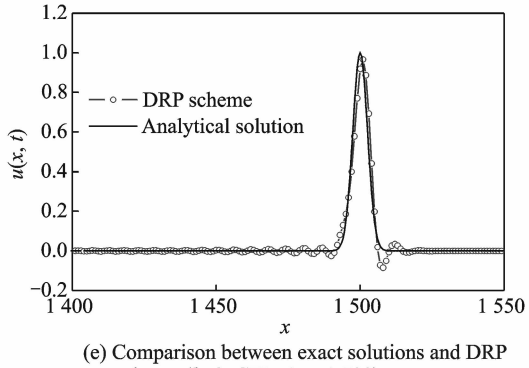

(e) Comparison between exact solutions and DRP scheme (b=3, CFL=1, t=1 500)

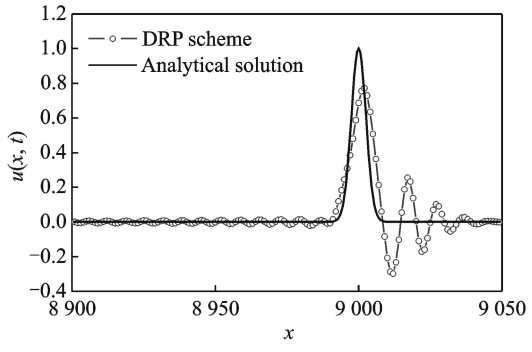

(f) Comparison between exact solutions and DRP scheme (b=3, CFL=1, t=9 000)

Fig. 5 Comparisons of numerical results for different numerical methods with the same order of 6

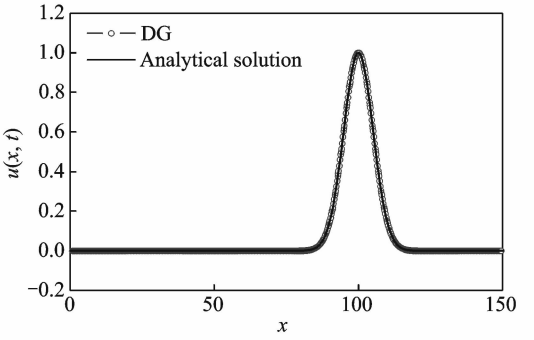

(a) Comparison between exact solutions and DG method (b=6, t=100)

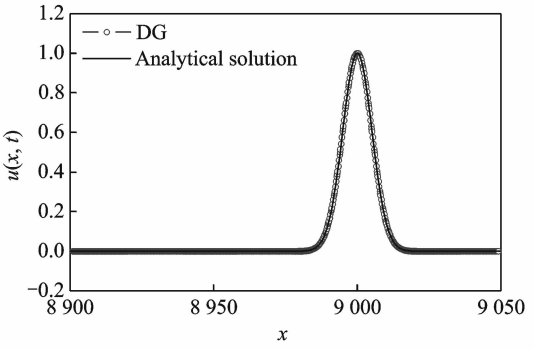

(b) Comparison between exact solutions and DG method (b=6, t=9 000)

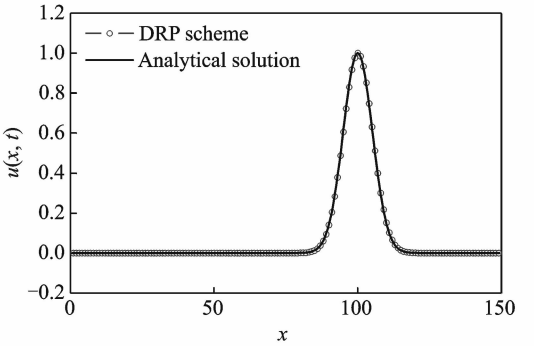

(c) Comparison between exact solutions and DRP scheme (b=6, CFL=1, t=100)

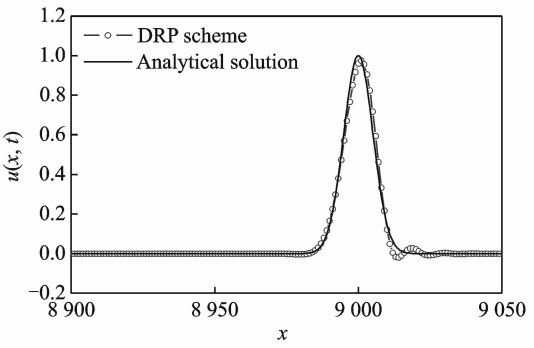

(d) Comparison between exact solutions and DRP scheme (b=6, CFL=1, t=9 000)

Fig. 6 Comparisons of numerical results for different numerical schemes with the same order of 6

Finally, to further evaluate the performance of the nodal DG method for short wave propagation, an initial disturbance wave with $b=0.5$ are investigated using this method. Fig. 8 presents the comparisons between the exact and computed

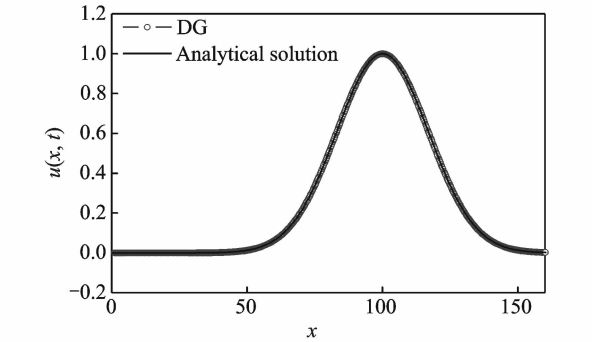

(a) Comparison between exact solutions and DG method (b=20, t=100)

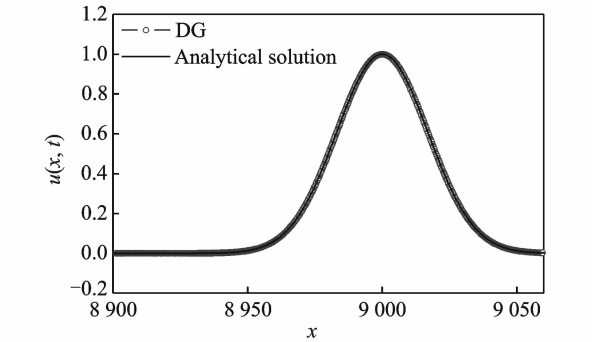

(b) Comparison between exact solutions and DG method (b=20, t=9 000)

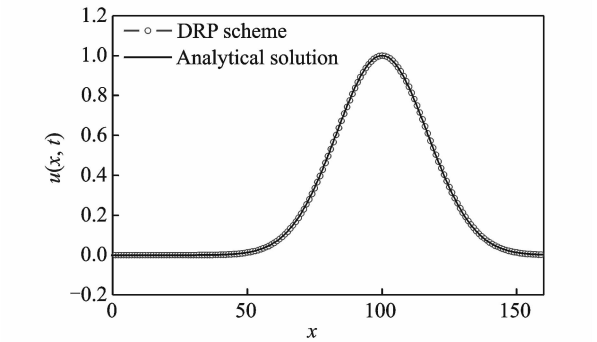

(c) Comparison between exact solutions and DRP scheme (b=20, CFL=1, t=100)

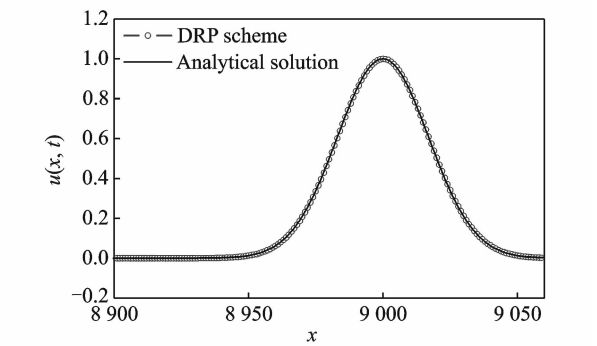

(d) Comparison between exact solutions and DRP scheme (b=20, CFL=1, t=9 000)

Fig. 7 Comparisons of numerical results for different numerical schemes with the same order of 6

results. It is easy to see that, for $b=0.5$, the nodal DG scheme initially produces lower error level shown in Fig. 8(a). At time progresses (t=4 000), dispersion becomes visible while dissipation becomes gradually obvious shown in Fig. 8(b), which indicate that the wave number of physics wave excess the solvable wave number range of nodal DG method.

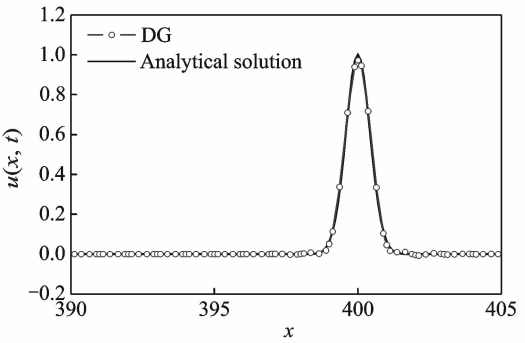

(a) b=0.5, t=400

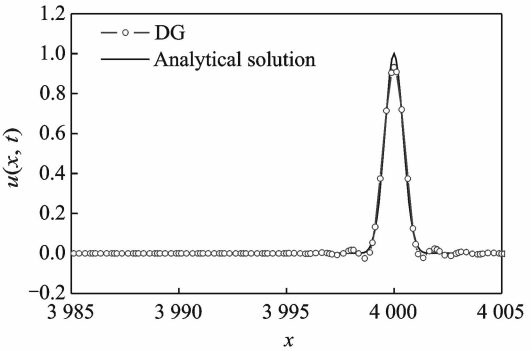

(b) b=0.5, t=4 000

Fig. 8 Comparisons between exact solutions and that of DG method with the order of 6

Example 2 Initial disturbance consisting of rectangular profile is

$$u(x,0)=0.5[H(x+50)-H(x-50)] \tag{13}$$

where $H(x)$ is the Heaviside function.

In this paper, authors study the performance of the DG method in rectangular wave. Moreover, numerical results among the nodal DG method, the seven-point stencil DRP scheme and the five-point 6th order compact scheme combined with the 4th order four-stage Runge-Kutta method are compared.

Figs. 9 — 11 show the comparisons between the numerical results obtained using nodal DG method, DRP scheme and compact scheme and the exact case at dimensionless time $t=50$ respectively, where the solid lines represent the exact case and the circle lines represent numerical re-

sults. In Fig. 9, the numerical solution obtained using nodal DG method with a pure central flux has obviously high frequency oscillations shown in Fig. 9(a), which looks like the same as those of finite difference type scheme without artificial selective damping shown in Figs. 10(a, c). The spurious waves of the computed solution are generated by the discontinuities of the initial condition.

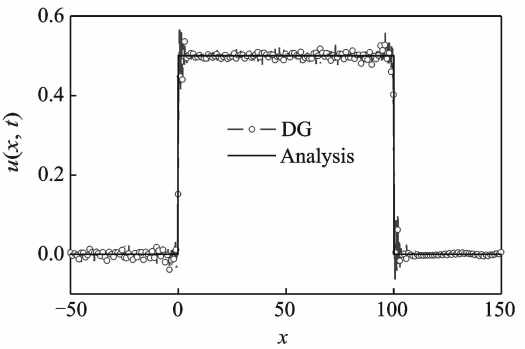

(a) With a central flux

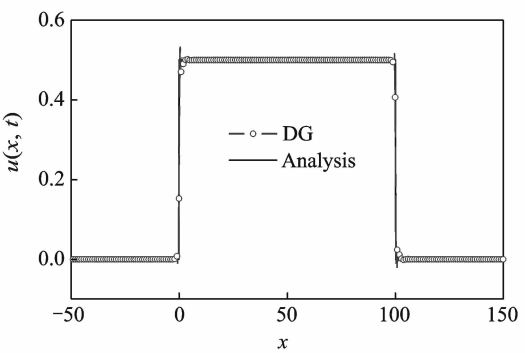

(b) With an upwind flux

Fig. 9 Comparisons between the computed and exact solutions ($t=50$)

The grid-to-grid oscillations have the highest group velocity. If an upwind flux is used, unphysical oscillations except for near the discontinuous location are eliminated effectively, as shown in Fig. 9(b). Therefore, a technique to eliminate possible spurious oscillations at the discontinuous location without any effect on smooth region is needed. For finite difference type schemes, if the artificial selective damping terms, described by Ref. [21], are added to the advection Eq. (1), the unphysical oscillations are largely removed, as shown in Figs. 10(b, d). For the nodal DG method, if a TVBM slope limiter described by Ref. [12] is introduced, the unphysical oscillations are almost completely eliminated as shown in Fig. 11. The quality of the computed solution

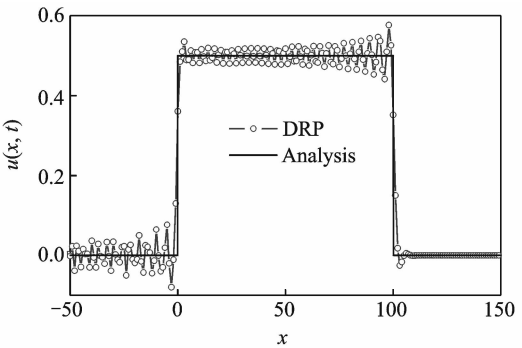

(a) Comparison between exact solutions and DRP scheme without artificial selective damping

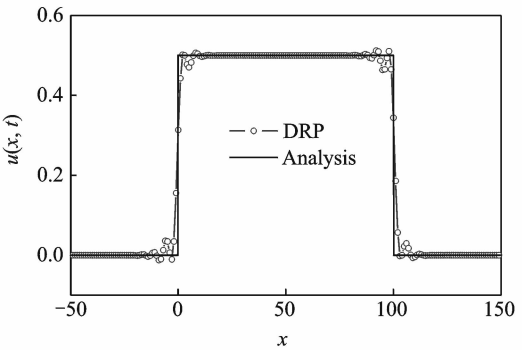

(b) Comparison between exact solutions and DRP scheme with artificial selective damping

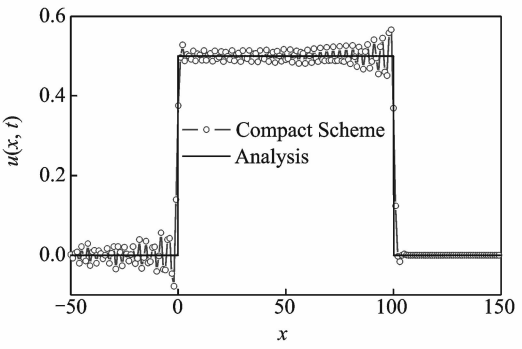

(c) Comparison between exact solutions and compact scheme without artificial selective damping

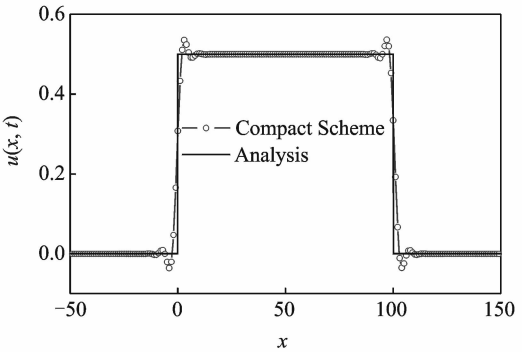

(d) Comparison between exact solutions and compact scheme with artificial selective damping

Fig. 10 Comparisons between the computed and the exact solutions ($t=50$)

is greatly improved, which is even better as the grid length decreasing(Fig. 11(b)).

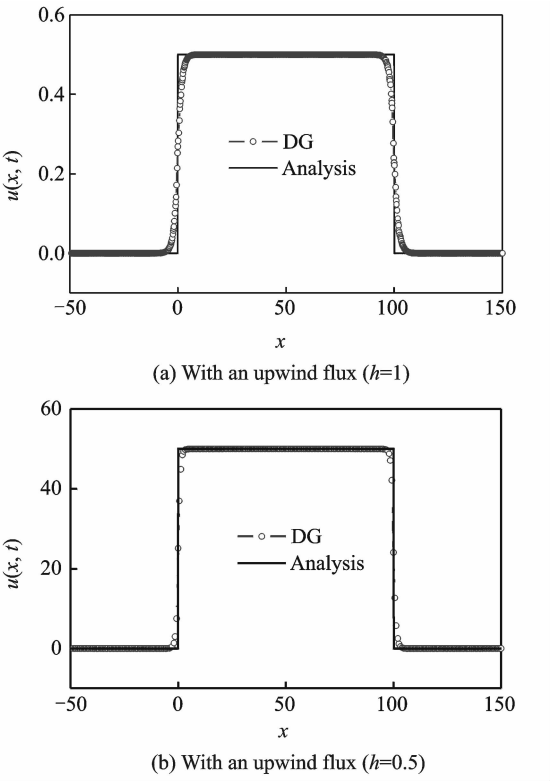

Fig. 11 Comparison between computed and exact solutions, with limiter $t=50$

4 Conclusions

A dispersion analysis of nodal DG method for the advection equation is investigated by utilizing an eigenvalue analysis. The present study shows that, with the same orders of scheme, the normalized maximum resolvable wave number of the nodal DG method is between those of the DRP scheme and compact scheme, and the number of points per wavelength of this method is less than those of modal DG method.

Two kinds of test problems of wave propagation with initial disturbance consisting of a Gaussian profile or rectangular pulse are investigated. The computed results indicate that the nodal DG method performs very well for short, intermediate, and long wave computation over the interval of time. However, DRP scheme may produce significant numerical dispersion and dissipation for a short wave, as well as small dispersion error for intermediate wave. For the initial disturbance with rectangular pulse, the nodal discontinuous Galerkin method with a pure central flux has obvious high frequency oscillations, which is the same as those obtained using finite difference type schemes without artificial selective damping. If an upwind flux is adopted, spurious waves are eliminated effectively except for the location of discontinuities. When a TVBM limiter is used, the spurious short waves are almost completely removed. The quality of the computed solution has greatly improved, which illustrates that this method is appropriate for simulating the acoustic wave propagation even including initial discontinuousness.

References:

[1] Hu F Q, Hussaini M Y, Manthey J L. Low-dissipation and low-dispersion Runge-Kutta schemes for computational acoustics[J]. J Comput Phys, 1996, 124:177-191.

[2] Tam C K W. Computational aeroacoustics: An overview of computational challenges and applications[J]. INT J Comput Fluid D, 2004,18:547-567.

[3] Tam C K W, Ishii K. Recent advances in computational aeroacoustics[J]. Fluid Dyn Res, 2006, 38: 591-615.

[4] Lele S K. Compact finite difference schemes with spectral-like resolution[J]. J Comput Phys, 1992, 103:16-42.

[5] Lele S K. Computational aeroacoustics: A review [R]. AIAA Paper 97-0018, 1997.

[6] Makridakis C, Monk P. Time-discrete finite element schemes for Maxwell's equations[J]. RAIRO Model Math Anal Numer, 1995,29:171-197.

[7] Delorme P, Mazet P, Peyret C, et al. Computational aeroacoustics applications based on a discontinuous Galerkin method[J]. Comptes Rendus Mecanique, 2005,333:676-682.

[8] Cockburn B, Shu C W. The Runge-Kutta local projection P1-discontinuous Galerkin method for scalar conservation laws[J]. RAIRO Model Math Anal, 1991(25):337-361.

[9] Cockburn B, Shu C W. TVB Runge-Kutta local projection discontinuous Galerkin finite element method for conservation laws Ⅱ: General framework[J]. Math Comp, 1989,52:411-435.

[10] Cockburn B, Lin S, Shu C W. TVB Runge-Kutta local projection discontinuous Galerkin finite element

method for conservation laws III: One-dimensional systems[J]. J Comput Phys, 1989,84:90-113.

[11] Cockburn B, Hou S, Shu C W. The Runge-Kutta local projection discontinuous Galerkin finite element method for conservation laws IV: The multidimensional case[J]. Math Comp,1990,54:545-581.

[12] Cockburn B, Shu C W. TVB Runge-Kutta discontinuous Galerkin method for conservation laws V: Multidimensional systems[J]. J Comput Phys, 1998, 141:199-224.

[13] Chevaugeon N, Xin J, Hu P. Discontinuous Galerkin methods applied to shock and blast problems[J]. J Sci Comput,2005,22:227-243.

[14] Qiu J X, Khoo B C, Shu C W. A numerical study for the performance of the Runge Kutta discontinuous Galerkin method based on different numerical fluxes [J]. J Comput Phys,2006,212:540-565.

[15] Hu F Q. Application of discontinuous Galerkin method to computational acoustics[R]. AIAA-99-3308, 1999.

[16] Hu F Q, Hussaini M Y, Rasetarineray P. An analysis of the discontinuous Galerkin method for wave propagation problems[J]. J Comput Phys,1999,151: 921-946.

[17] Hesthaven J S, Warburton T. Nodal discontinuous Galerkin methods: Algorithms, analysis, and applications[M]. Springer,2007.

[18] Hu F Q. A stable, perfectly matched layer for linearized Euler equations in unsplit physical variables[J]. J Comput Phys 2001,173:455-480.

[19] Hu F Q, Atkins H L. Eigensolution analysis of the discontinuous Galerkin method with nonuniform grids [J]. J Comput Phys, 2002,182:516-545.

[20] Popescu M, Shyy W. Assessment of dispersion-relation-preserving and space-time CE/SE schemes for wave equations[J]. Numerical Heat Transfer, Part B, 2002,42:93-118.

[21] Tam C K W. Computational aeroacoustics: Issues and methods[J]. AIAA Journal,1995,33:1788-1796.

(Executive editor: Zhang Tong)